

RHESSI Observations of a Simple Large X-ray Flare on 11-03-2003

Wei Liu¹, Yan Wei Jiang¹, Siming Liu¹, and Vahé Petrosian²

Center for Space Science and Astrophysics, Stanford University, Stanford, California 94305

ABSTRACT

We present data analysis and interpretation of a simple X-class flare observed with *RHESSI* on November 3, 2003. In contrast to other X-class flares observed previously, this flare shows a very simple morphology with well defined looptop (LT) and footpoint (FP) sources. The almost monotonic upward motion of the LT source and increase in separation of the two FP sources are consistent with magnetic reconnection models proposed for solar flares. In addition, we find that the source motions are relatively slower during the more active phases of hard X-ray emission; the emission centroid of the LT source shifts toward higher altitudes with the increase of energy; the separation between the LT emission centroids at two different photon energies is anti-correlated with the FP flux. Non-uniformity of the reconnecting magnetic fields could be a possible explanation of these features.

Subject headings: acceleration of particles—Sun: flares—Sun: X-rays

1. Introduction

With its high temporal, spatial, spectral resolution and broad energy coverage, the *Reuven Ramaty High Energy Solar Spectroscopic Imager* (*RHESSI*) has revealed many features of solar flares with unprecedented details (Lin et al. 2002). Since its launch on 5 February 2002, *RHESSI* has observed several X-class flares and thousands of mid-class and small flares. The compactness of microflares limits our access to details of the energy release and particle acceleration processes (Krucker et al. 2002). On the other hand large and well resolved flares usually involve multiple loops with complex structures and the looptop (LT) and associated footpoint (FP) sources are not readily identified and separated (Gallagher

¹Department of Physics; weiliu@sun.stanford.edu, arjiang@stanford.edu, liusm@stanford.edu

²Departments of Physics and Applied Physics; vahe@astronomy.stanford.edu

et al. 2002; Lin et al. 2003). This makes a direct comparison of theoretical models with observations a challenging task (Alexander & Metcalf 2002; Sui et al. 2002). This task would be easier for a large flare with a simple morphology, where one can identify source positions and evolutions with certainty (Tsuneta et al. 1992; Tsuneta 1996; Tsuneta et al. 1997).

In late October and early November 2003, *RHESSI* and other instruments observed a series of X-class flares from solar active regions AR 0486 and 0488 (reminiscence of the June 1991 flares of the previous solar cycle; Schmieder et al. 1994). Among these flares, we studied an event which occurred on November 3 in AR 0488 at heliographic coordinate N09° W77°. Unlike other X-class flares, e.g. the April 21, 2002 flare (Gallagher et al. 2002) and the gamma-ray flare on July 23, 2002 (Lin et al. 2003), this flare shows a surprisingly simple morphology with well defined LT and two FP sources.

In this letter we present a brief description of the spatial evolution of the various emission regions of this flare. As we will show this provides an excellent example of the classical solar flare model of magnetic reconnection and energy release in an inverted Y magnetic field configuration (Kopp & Pneuman 1976; Forbes & Acton 1996; Aschwanden 2002), whereby reconnection in the oppositely directed field lines leads to particle acceleration near the LT. The energy release and particle acceleration processes are not well understood, nevertheless, it is expected that the reconnection will produce closed loops at lower altitudes first and progress to higher overlying loops as time advances. Consequently, the altitude of the LT source and the separation of the two FPs should increase with time. The flare studied here shows this exact behavior.

On the other hand, we also see evidence for deviations from the simplest reconnection models. Our study indicate that the reconnecting fields could be nonuniform and may have a shearing component. In the next section, we present the observations, data analysis, and our results. Their implications are discussed in § 3.

2. Observations and Data Analysis

The flare under study, classified as a *GOES* X3.9 class flare, was observed by *RHESSI*, *Solar and Heliospheric Observatory (SOHO)*, etc. Figure 1a shows the *RHESSI* light curves. In lower energy channels (< 25 keV), the count rates started to rise at around 09:43 UT, peaked about nine minutes later, and then began a monotonic declining phase till 10:01:20 UT when *RHESSI* entered the Earth's night region. The higher energy channel (> 50 keV) light curves exhibit two broad impulsive bursts, each of them consisting of several pulses, with a more quiescent part in between, suggesting a persistent but episodic energy release

process. Impulsive radio activities were also observed by the Nançay Observatory (Vilmer, private communication). A partial halo Coronal Mass Ejection (CME) with a speed of ~ 1375 km/s was observed by the Large Angle and Spectrometric Coronagraph on *SOHO*.

To study the hard X-ray (HXR) source motion and structure, we obtained images at different energies in 20-second intervals from 09:46:20 through 10:01:00 UT using the CLEAN algorithm (Hurford et al. 2002) and front segments of detectors 3-8 to achieve a FWHM of $9''.8$ with a $0''.5$ pixel size. Figure 2 shows the HXR emission contours during the two main activity peaks. There are three sources: a LT, a Northern FP (N-FP), and a Southern FP (S-FP). The LT source dominates at lower energy while the FPs dominate the higher energy emission. As evident from the background pre-flare magnetogram obtained with the Michelson Doppler Imager (MDI), the N-FP is around a negative magnetic polarity region while the S-FP remains in a region of positive polarity. Note that early in the event there is a partial overlap between the N-FP and the LT source. Grids with higher spatial resolution will not help for this flare because grid 2 has severely degraded conditions (Smith et al. 2002) and grid 1 will over-resolve the sources (See Schmahl & Hurford 2003 for technical details). A post-flare (10:35:43 UT) Extreme ultraviolet Imaging Telescope (EIT) 195 Å image (not shown) shows a loop structure which agrees well with the *RHESSI* sources.

As shown in Figure 2 the LT and FPs have well defined and correlated motions, with the symbols indicating their emission centroids at different times. The yellow dashed line represents the main direction of the LT motion, which is roughly at a right angle to the solar limb. We refer to the motion along this direction as changes in altitude. The motion perpendicular to this direction might be due to asymmetry of the reconnecting loops or LT motion along an arcade. Before the rise of impulsive HXR emission, there is an apparent downward LT motion. This downward motion could indicate a shrinkage of newly formed loops. It may also be due to formation of nearby sources (Krucker, Hurford, & Lin 2003), or due to projection effects should the LT source moves eastward along arcades of loops (Sato 2001). Qualitatively similar features have been seen in several other flares (Krucker et al. 2003; Sui & Holman 2003), suggesting that this may be a common characteristic of solar flares. However, for the remainder of the flare duration the LT source rises systematically. The apparent separation of the FP sources, whenever detectable, also increases with comparable speed. As emphasized above, this is expected in a simple continuous reconnection process which moves up to the corona, accelerating particles and energizing plasma higher up into overlying larger loops.

To analyze the FP motion quantitatively, one needs to take into account projection effects because any motion and its associated uncertainty in the east-west direction are amplified by a factor of about $\csc 77^\circ \simeq 4.4$. Motions in this direction are highly uncertain

and the motion of both FPs appears to have an east-west component. Magnetic reconnection, on the other hand, is characterized by the change in the size of newly formed loops rather than their absolute motions. Thus one may concentrate on the relative motion of the two conjugate FPs. In the insert panel of Figure 2, we illustrate this relative motion by fixing the S-FP at the origin of the coordinates and showing the relative locations of the N-FP. The relative motion is obviously systematic. The fact that the line tracing the location of the N-FP is not exactly aligned with the lines connecting the two FPs shows that there is another component of the relative motion introducing a small rotation of the plane containing the newly formed loop. Because this line is nearly parallel to the longitudinal line, one can ignore the projection affects. We will quantify the relative motion along this line and the standard deviation of the displacement (apparently) perpendicular to this line will be used as an upper limit for the uncertainties of this relative motion.

Figure 1b shows this relative motion of the FPs (in 50-71 keV) along with the location of the emission centroids of the LT source in three energy bands projected onto its main direction of motion. As evident, the two motions are correlated and the two set of data points are nearly parallel to each other indicating comparable velocities. To further investigate these motions we divide the observed flare duration into four phases: a pre-impulsive phase (before 09:48:10 UT) when there is no significant high energy HXR emission, a rising phase (from 09:48:10 to 09:49:50 UT), a declining phase (from 09:49:50 to 09:56:50 UT), and a second active phase (from 09:56:50 till 10:01:00 UT). We then fit straight lines to each segment and determine the corresponding average velocities. The results are summarized in Table 1. Surprisingly, the LT velocity is highest in the declining phase, when the X-ray emission is relatively weaker (Fig. 1c). In the simplest model of reconnection of *uniform* and oppositely directed magnetic fields, one would expect the opposite correlation, i.e. a higher rate of energy release when the velocity is larger. However, this would be true if the observed HXR flux were actually proportional to the total energy release and if reconnection were indeed occurring in a uniform background plasma, neither one of which is exactly true.

Another interesting morphological evolution is the change of the centroid of the LT source with energy. In Figure 3 we show the *RHESSI* 75% contours and centroids at several energies superposed on an MDI continuum image showing sunspots. Compared with the two FPs, the LT source shows a clear and systematic displacement of the centroid of the higher energy emissions toward higher altitudes, as seen in two other flares (Sui & Holman 2003; Gallagher et al. 2002). To investigate what this separation of the LT centroids is related to, we looked for its correlations with other characteristics. We found an anti-correlation between the centroid separation and the high energy (100-300 keV) count rate, which comes mainly from the FPs (Fig. 1d). The continuous curve in Figure 4 shows their cross-correlation function, which gives a peak correlation coefficient of -0.51 ± 0.08 with a

time lag of $\Delta t = -22 \pm 39$ s. The data points (LT separation vs HXR count rate) used for evaluating the correlation and a straight-line fit are also shown in the same figure.

3. Discussion

We have investigated the November 3, 2003 X3.9 flare, having a simple morphology with well defined LT and FP sources. The high flux combined with the simple loop structure allows us to determine the spatial evolution of the LT and FP sources clearly and to compare with the simple reconnection models. Similar studies of flares have been limited to the investigation of the motion of the FPs alone (Sakao, Kosugi & Masuda 1998; Qiu et al. 2002; Fletcher & Hudson 2002) or have dealt with complex loop structures (Krucker et al. 2003; Qiu, Lee & Gary 2003). This has made the comparison with models more difficult. Our analysis of *RHESSI* data has yielded several new and interesting results.

1. We observe a systematic rise of the LT source and a comparable increase in the separation of the FPs as the flare proceeds. This agrees very well with the canonical solar flare model of magnetic reconnection in an inverted Y configuration. Similar behaviors have been reported previously using soft X-ray or EUV observations (Švestka et al. 1987; Tsuneta et al. 1992; Gallagher et al. 2002) during later thermal gradual phases of flares. However, these emissions are not directly related to the impulsive particle acceleration processes (Forbes & Acton 1996).
2. The LT source seems to move more slowly during the HXR peaks than during the declining and more quiescent phases, in apparent disagreement with reconnection of *uniform* and oppositely directed field lines, where one would expect a correlation between the velocity of the LT source and the energy release rate. However, we note that the HXR flux is not a good proxy for the energy release rate and the magnetic fields in the reconnection region are likely to be nonuniform. Stronger magnetic fields would require smaller volume of reconnecting fields and possibly slower motion. However, in an inhomogeneous case other factors like the geometry and Alfvén velocity variation can also come into play. This problem needs further exploration.
3. The centroid of the LT source appears to be at higher altitudes for higher photon energies. This suggests that the energy releasing process happens above the LT and that harder spectra, implying more efficient acceleration, are produced at higher altitudes. In the stochastic acceleration model by turbulence where the acceleration efficiency depends on the intensity of turbulence, this would indicate a decrease of the intensity

with decreasing altitudes, presumably due to decay of turbulence away from its source at a higher altitude.

4. The above shift of the centroids decreases with the increase of HXR flux from the FPs. Such an anti-correlation will be difficult to produce in simple models. In the above mentioned model, this would imply a more homogeneous distribution of turbulence during more active phases.

Acknowledgments

The work is supported by NASA grants NAG5-12111, NAG5 11918-1, and NSF grant ATM-0312344. We are indebted to S. Krucker for numerous help and for valuable comments as a referee. We also would like to thank T. Metcalf, G. Hurford for helpful discussions and suggestions, and are grateful to K. Tolbert, R. Schwartz, and J. McTiernan for their help with analyzing *RHESSI* data.

REFERENCES

- Alexander, D., & Metcalf, T. R. 2002, *Sol. Phys.*, 210, 323
- Aschwanden, M. J. 2002, *Space Science Reviews*, 101, 1
- Emslie, A. G., Kontar, E. P., Krucker, S., & Lin, R. P. 2003, *ApJ*, 595, L107
- Fletcher, L., & Hudson, H. S. 2002, *Sol. Phys.*, 210, 307
- Forbes, T. G., & Acton, L. W. 1996, *ApJ*, 459, 330
- Gallagher, P. T., Dennis, B. R., Krucker, S., Schwartz, R. A., & Tolbert, A. K. 2002, *Sol. Phys.*, 210, 341
- Holman, G. D., Sui, L., Schwartz, R. A., Emslie, A. G. 2003, *ApJ*, 595, L97
- Hurford, G. J., et al. 2002, *Sol. Phys.*, 210, 61
- Kopp, R. A., & Pneuman, G. W. 1976, *Sol. Phys.*, 50, 85
- Krucker, S., Christe, S., Lin, R. P., Hurford, G. J., & Schwartz, R. A. 2002, *Sol. Phys.*, 210, 445
- Krucker, S., Hurford, G. J., & Lin, R. P. 2003, *ApJ*, 595, L103

- Lin, R. P., et al. 2002, *Sol. Phys.*, 210, 3
- Lin, R. P., et al. 2003, *ApJ*, 595, L69
- Petrosian, V., Donaghy, T. Q., & McTiernan, J. M. 2002, *ApJ*, 569, 459
- Qiu, J., Lee, J., Gary, D. E., & Wang, H. 2002, *ApJ*, 565, 1335
- Qiu, J., Lee, J., & Gary, D. E. 2003, *ApJ*, In press
- Sakao, T., Kosugi, T., & Masuda, S. 1998, in *ASSL Vol. 229, Observational Plasma Astrophysics: Five Years of *Yohkoh* and Beyond*, ed. T. Watanabe, T. Kosugi, & A. C. Sterling (Boston: Kluwer), 273
- Sato, J. 2001, *ApJ*, 558, L137
- Schmahl, E. J., & Hurford, G. J. 2002, *Sol. Phys.*, 210, 273
- Schmahl, E. J., & Hurford, G. J. 2003, *Advances in Space Research*, 32, 2477
- Schmieder, B., et al. 1994, *Sol. Phys.*, 150, 199
- Smith, D. M., et al. 2002, *Sol. Phys.*, 210, 33
- Sui, L., Holman, G. D., Dennis, B. R., Krucker, S., Schwartz, R. A., & Tolbert, K. 2002, *Sol. Phys.*, 210, 245
- Sui, L., & Holman, G. D. 2003, *ApJ*, 596, L251
- Švestka, Z. F., Fontenla, J. M., Machado, M. E., Martin, S. F., Neidig, D. F., & Poletto, G. 1987, *Sol. Phys.*, 108, 237
- Tsuneta, S., Hara, H., Shimizu, T., Acton, L. W., Strong, K. T., Hudson, H. S., & Ogawara, Y. 1992, *PASJ*, 44, L63
- Tsuneta, S. 1996, *ApJ*, 456, 840
- Tsuneta, S., Masuda, S., Kosugi, T., & Sato, J. 1997, *ApJ*, 478, 787

Table 1: LT velocities and FP separation speed.

| Time range (UT) | LT velocities (km/s) | | | | FP speed(km/s) (50-71 keV) |
|--------------------|----------------------|-----------------|-----------------|-----------------|-------------------------------|
| | 9-12 keV | 12-15 keV | 15-19 keV | 19-24 keV | |
| 09:46:20-09:48:10 | -18.3 ± 3.7 | -22.5 ± 4.6 | -32.5 ± 4.1 | -30.8 ± 4.7 | — — — |
| 09:48:10-09:49:50 | 3.5 ± 3.3 | 4.0 ± 3.0 | 4.7 ± 2.6 | 4.3 ± 2.7 | 29.1 ± 11.6 |
| 09:49:50-09:56:50 | 14.6 ± 0.4 | 16.5 ± 0.2 | 18.0 ± 0.2 | 20.9 ± 0.1 | 22.4 ± 2.5 |
| 09:56:50-10:01:00 | 9.3 ± 0.9 | 8.6 ± 0.7 | 6.6 ± 0.7 | 5.9 ± 0.5 | 10.4 ± 3.6 |

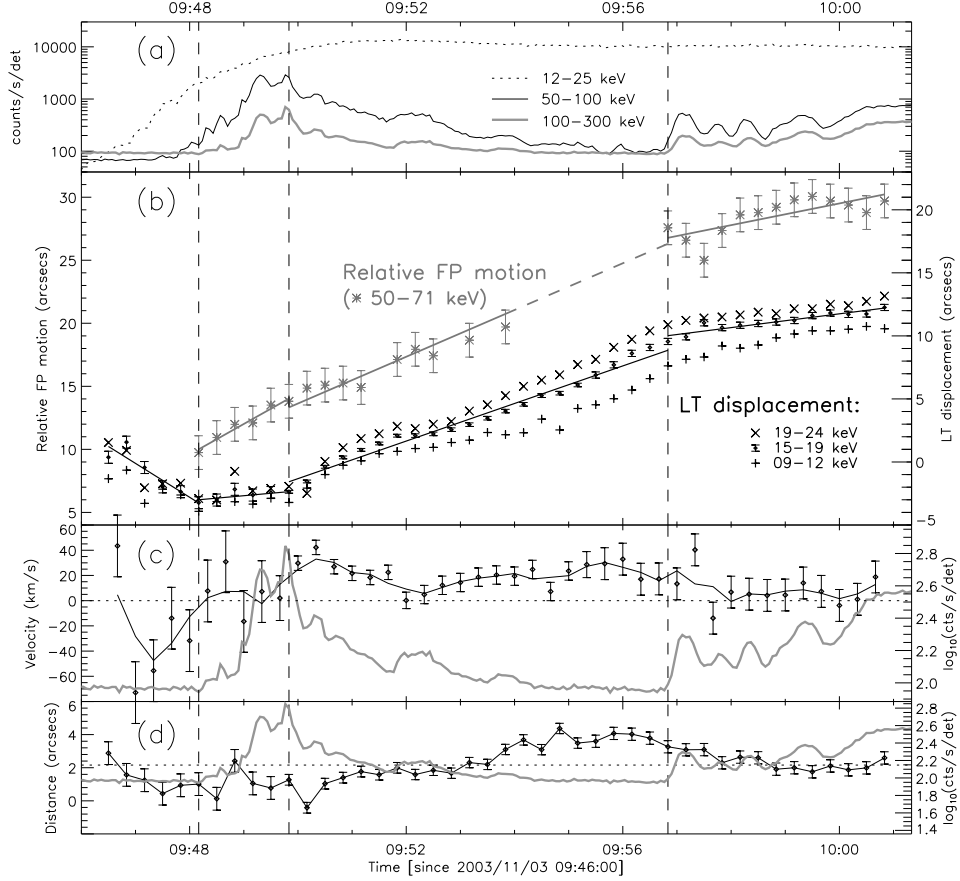


Fig. 1.— (a) *RHESSI* light curves (counts/second/detector). (b) The evolution of the altitude of the LT centroid (right scale) and the separation of the two FPs (left scale). The LT altitude here refers to the displacement along the main direction of motion which is nearly perpendicular to the solar limb. The straight lines are fits to the FP separation and LT altitude in 15-19 keV with vertical dashed lines separating the four phases as described in the text. The uncertainty of the centroid location in 15-19 keV is shown with the vertical error bars, which are similar to those in 9-12 keV and 19-24 keV (not shown). The uncertainty of the relative FP motion is also indicated. (c) The corresponding LT velocity in 15-19 keV. The thin curve is the velocity smoothed over 1-minute intervals. The thick grey curve is the logarithm of the 100-300 keV count rate (right scale). (d) Separation of the LT centroids in 19-24 keV and 9-12 keV (panel b) as a function of time. The dotted horizontal line marks the mean of this separation and the logarithm of the count rate (same as panel c).

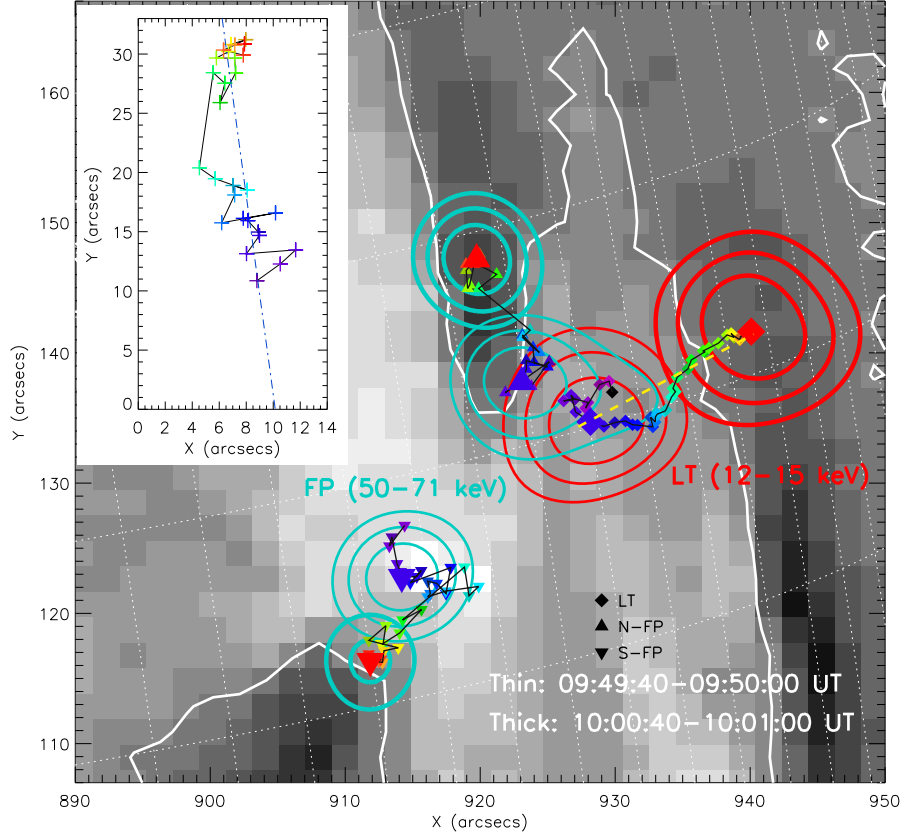


Fig. 2.— Temporal evolution of HXR source centroids, over-plotted on an MDI magnetogram (09:32:30 UT). Black line segments connect the centroids obtained from CLEAN images in successive 20-s intervals chronologically from black (09:46:20 UT) through violet, blue, green, yellow, and to red (10:01:00 UT). The LT (12-15 keV) centroid is the brightness-weighted source center within the 70% level contour but each FP (50-71 keV) centroid is the peak position obtained with a 3×3 -pixel parabolic fit around the brightest pixel. The yellow dashed line represents the main direction of motion of the LT source. To estimate the uncertainty in the LT centroid location, we fitted the LT data points with 4 straight lines within the time intervals, 09:46:20-09:49:40 UT, 09:49:40-09:52:00 UT, 09:52:00-09:55:20 UT, and 09:55:20-10:01:00 UT, respectively. For each interval, following Krucker et al. (2003), the standard deviation of the offset of the data from the corresponding straight line was used as the error in the location. The insert shows the relative positions of the N-FP with respect to the S-FP which is fixed at the origin. We attribute the motion perpendicular to the straight line to uncertainties in the locations (see text for details). Four HXR images in two time intervals, 09:49:40-09:50:00 UT (thin) and 10:00:40-10:01:00 UT (thick), and in two energy channels, 12-15 keV (red) and 50-71 keV (cyan), are over-plotted as contours (at 55, 70, 85% levels of the maximum brightness of the image), which clearly depict the LT and FPs, respectively. The centroids corresponding to these two intervals are indicated with larger symbols. The magnetogram shows the line-of-sight magnetic field in a grey scale ranging from -979 (black: pointing away from the observer) to $+1004$ (white) Gauss. The apparent neutral lines are marked in white.

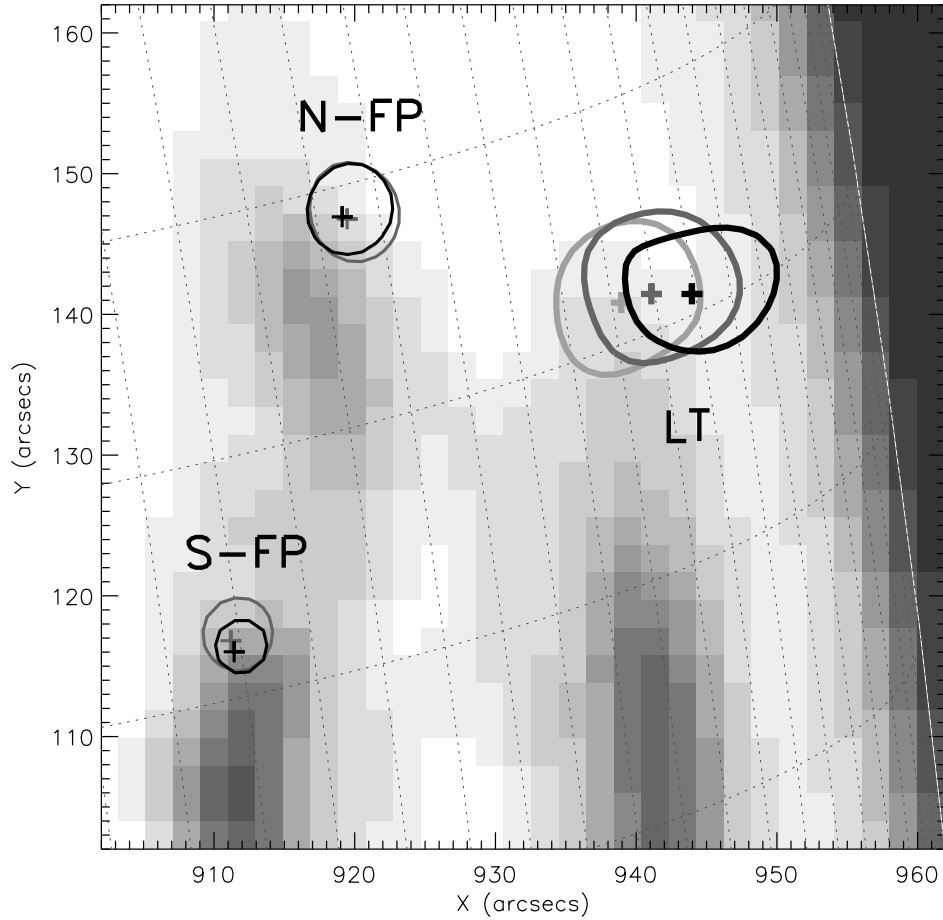


Fig. 3.— *RHESSI* image contours (75%) and the corresponding brightness-weighted centroids (+) in the interval 10:01:00-10:01:20 UT. The LT contours are for 12-14 keV (light grey), 18-21 keV (grey), and 27-31 keV (dark) and the FP contours are for 40-46 keV (grey) and 60-73 keV (dark). The background is an MDI continuum map taken at 09:36:00 UT. The dark areas inside the limb are three sunspots.

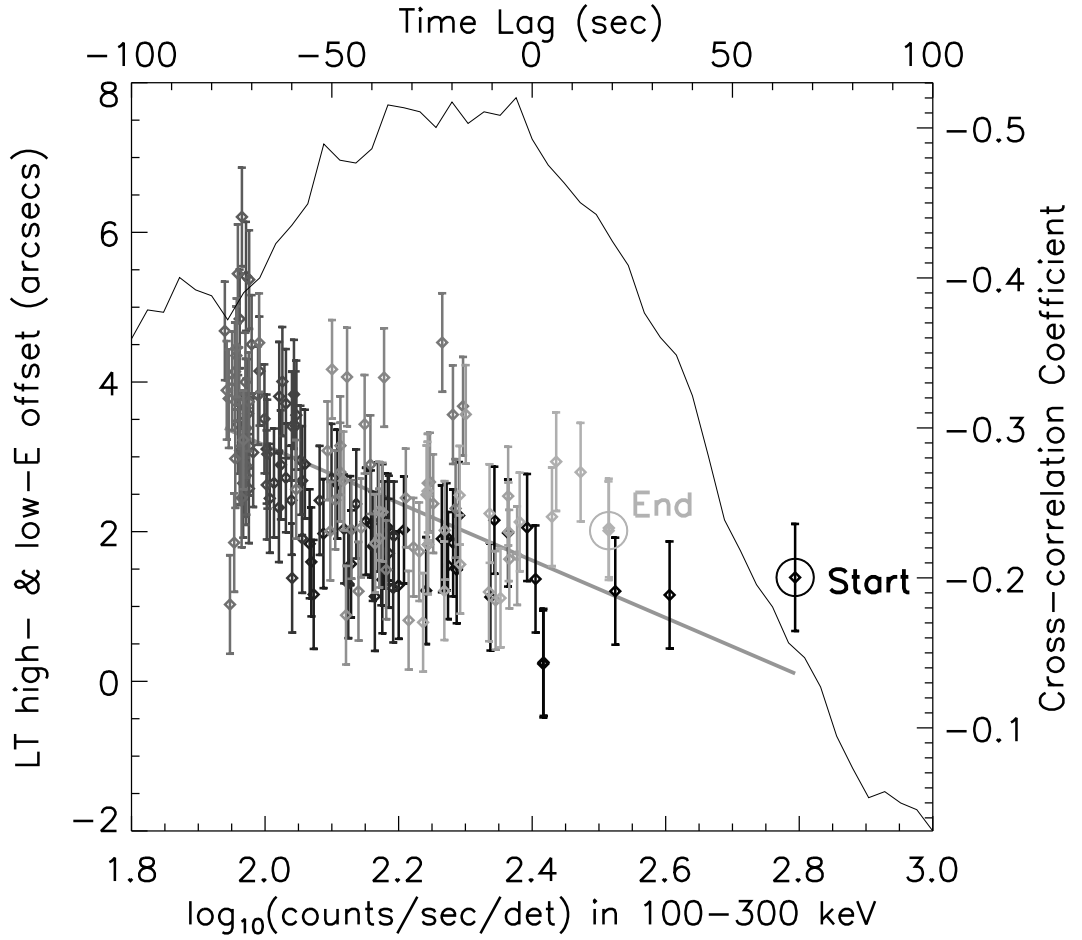


Fig. 4.— Correlation between the LT structure and the 100-300 keV (mainly FPs) light curve. The thin curve (with the top and right axis) shows the cross-correlation coefficient of the logarithm of the count rate and the separation between the 19-24 keV and 9-12 keV centroids of the LT source, showing a 22 ± 39 s delay relative to the light curve. The separation is similar to that shown in Figure 1d but with a higher time resolution, obtained by imaging at a 4-s cadence (same as the light curve) with an integration time of one spacecraft spin period (~ 4 s) from 09:49:48 to 10:01:00 UT. We excluded the first two phases of the flare duration when the spatial contamination to the LT source by the N-FP is severe. The diamond symbols (with the bottom and left axis) show the LT separation versus the logarithm of the count rate shifted by +24 seconds, corresponding to the peak of the correlation coefficient. The vertical error bars represent the uncertainty in the centroid separation. The darkness of the symbols represents time with the start and end point being circled. The grey thick line is a linear fit to the data with a slope of -3.84 ± 0.34 .